General Theory for Longitudinal Nonreciprocal Charge Transport

Hong Jian Zhao,[1] Lingling Tao,[2,*] Yuhao Fu,[1,†] Laurent Bellaiche,[3,4] and Yanming Ma[1,5,6,‡]

[1]*Key Laboratory of Material Simulation Methods and Software of Ministry of Education, College of Physics, Jilin University, Changchun 130012, China*

[2]*School of Physics, Harbin Institute of Technology, Harbin 150001, China*

[3]*Smart Ferroic Materials Center, Physics Department and Institute for Nanoscience and Engineering, University of Arkansas, Fayetteville, Arkansas 72701, USA*

[4]*Department of Materials Science and Engineering, Tel Aviv University, Ramat Aviv, Tel Aviv 6997801, Israel*

[5]*International Center of Future Science, Jilin University, Changchun 130012, China*

[6]*State Key Laboratory of Superhard Materials, College of Physics, Jilin University, Changchun 130012, China*

(Received 28 March 2024; revised 24 June 2024; accepted 11 July 2024; published 29 August 2024)

The longitudinal nonreciprocal charge transport (NCT) in crystalline materials is a highly nontrivial phenomenon, motivating the design of next generation two-terminal rectification devices (e.g., semiconductor diodes beyond PN junctions). The practical application of such devices is built upon crystalline materials whose longitudinal NCT occurs at room temperature and under low magnetic field. However, materials of this type are rather rare and elusive, and theory guiding the discovery of these materials is lacking. Here, we develop such a theory within the framework of semiclassical Boltzmann transport theory. By symmetry analysis, we classify the complete 122 magnetic point groups with respect to the longitudinal NCT phenomenon. The symmetry-adapted Hamiltonian analysis further uncovers a previously overlooked mechanism for this phenomenon. Our theory guides the first-principles prediction of longitudinal NCT in multiferroic ε-Fe_2O_3 semiconductor that possibly occurs at room temperature, without the application of external magnetic field. These findings advance our fundamental understandings of longitudinal NCT in crystalline materials, and aid the corresponding materials discoveries.

DOI: 10.1103/PhysRevLett.133.096802

Introduction—Nonreciprocal charge transport (NCT) is a phenomenon for which a material with oppositely flowed electric currents exhibits unequal resistances [1–3]. This phenomenon naturally occurs in semiconductor PN junctions, and yields two-terminal junction diodes as the building blocks in modern electronics [2–5]. Recent work indicates that crystalline materials with broken inversion and time-reversal symmetries (e.g., noncentrosymmetric semiconductors [5–9], metallic magnets [10,11], and topological materials [12–15]) may host NCT as well [3,16]. Such an NCT in crystalline materials is comprised of a transversal part and a longitudinal part [10,17]. The latter is reminiscent of the magnetochiral anisotropy effect [3,12,15,18,19], and opens an entirely new route to design novel two-terminal rectification devices (see, e.g., Refs. [5,6,14,20]). For instance, the longitudinal NCT in crystalline semiconductors motivates the design of next-generation semiconductor diodes, resembling the diodes based on PN junctions but without involving any junction [5,6,14,20]. Designing such devices and enabling their practical applications rely on crystalline materials with longitudinal NCT at room temperature and under low magnetic field, while these types of materials are rare and elusive. To guide materials discovery, a theory capturing the essential physics of longitudinal NCT in crystalline materials is of high necessity. But, unlike the case of PN junctions, the longitudinal NCT phenomena in crystals are rather complicated [3,5]—the aforementioned theory remaining lacking.

Here, we develop a general theory for longitudinal NCT [21] in ferromagnetic, antiferromagnetic, and nonmagnetic crystalline materials, within the framework of Boltzmann transport theory. We perform symmetry analysis and provide a classification of the complete 122 magnetic point groups (MPGs) regarding longitudinal NCT. Specifically, we identify 42 MPGs that host *intrinsic* longitudinal NCT (without involving magnetic field), where the longitudinal NCT stems from the magnetic order parameter. This resembles the magnetochiral anisotropy effect demonstrated in, for instance, Refs. [3,12,18,19]. We also find 20 MPGs that accommodate the extrinsic longitudinal NCT induced by external magnetic field, namely, the magnetochiral anisotropy effect. The longitudinal NCT in crystalline materials is further illustrated by constructing effective Hamiltonians. The effective Hamiltonian analysis helps to identify a previously overlooked mechanism responsible for the longitudinal NCT. Motivated by the design of

*Contact author: lltao@hit.edu.cn
†Contact author: yuhao_fu@jlu.edu.cn
‡Contact author: mym@jlu.edu.cn

intrinsic semiconductor diodes and guided by our theory, we predict by first-principles simulations that multiferroic ε-Fe_2O_3 semiconductor showcases intrinsic longitudinal NCT occurring at room temperature.

The longitudinal NCT from second-order nonlinear charge current—To begin with, we briefly overview the magneto-chiral anisotropy effect in crystalline materials (see, e.g., Refs. [3,12,18,19]). Under an external magnetic field B, a crystalline material with electric current I gains an unidirectional magnetoresistance $R(B,I)=\xi BI$ [3,5,18,19,22,23]. The sign of $R(B,I)$ is reversed by flipping I or B, and this corresponds to the NCT phenomenon. In the following, we shall demonstrate that such an NCT phenomenon generally occurs in materials with a spontaneous or induced magnetic order parameter L (e.g., magnetization or Néel vector), where L plays the role as B in $R(B,I)=\xi BI$.

Under relaxation time (τ) approximation, nonlinear Drude (τ^2 dependence) [3,10,24] and quantum metric (τ^0 dependence) [14,15] are two possible mechanisms for longitudinal NCT—Berry curvature dipole merely contributing transverse transport and being irrelevant to longitudinal NCT [15,25]. The nonlinear Drude is associated with effective masses and group velocities of Bloch electrons [5,6,10,11]. Yet, the quantum metric is ascribed to the interband Berry connection [14,15]. Such a mechanism remained long hidden and was only recently revealed by two seminal works [14,15]. Despite their different microscopic origins, the symmetry restrictions for the nonlinear Drude and quantum metric contributed longitudinal NCT are identical [15]. In this Letter, we focus on longitudinal second-order nonlinear Drude conductivity and perform symmetry analysis accordingly. This simplifies our discussion and enables the generalization of our symmetry arguments to the quantum metric contributed longitudinal NCT (see the *symmetry analysis* section). Under a direct electric field, the longitudinal second-order charge current density $J_\alpha^{(2)}$ is expressed as [10]

$$J_\alpha^{(2)}=\frac{e^3\tau^2E_\alpha^2}{8\pi^3\hbar^3}\sum_n\iiint\frac{\partial^2\epsilon_n}{\partial k_\alpha^2}\frac{df_0(\epsilon_n)}{d\epsilon_n}\frac{\partial\epsilon_n}{\partial k_\alpha}d^3\mathbf{k},\qquad(1)$$

where $\epsilon_n(\mathbf{k})\equiv\epsilon_n$ is the band dispersion, $\mathbf{k}\equiv k_\alpha\boldsymbol{\alpha}+k_\beta\boldsymbol{\beta}+k_\gamma\boldsymbol{\gamma}$ the wave vector ($\boldsymbol{\alpha}$, $\boldsymbol{\beta}$, and $\boldsymbol{\gamma}$ being three orthogonal unit vectors), n the band index, $\hbar$ the reduced Planck constant, e the elementary charge, $f_0(\epsilon_n)$ the Fermi-Dirac distribution at ϵ_n, and E_α the electric field along α direction (see e.g., Refs. [5,6,10,11,14,15] and Sec. I of the Supplemental Material [26] which includes Refs. [27–54] as well).

To show that $J_\alpha^{(2)}$ arises from the asymmetric band dispersion [3,10,24], we consider a symmetry operation that transforms $\mathbf{k}=k_\alpha\boldsymbol{\alpha}+k_\beta\boldsymbol{\beta}+k_\gamma\boldsymbol{\gamma}$ to $\mathbf{k}'=-k_\alpha\boldsymbol{\alpha}+\tilde{\kappa}_\beta\boldsymbol{\beta}+\tilde{\kappa}_\gamma\boldsymbol{\gamma}$, such that $\epsilon_n(k_\alpha\boldsymbol{\alpha}+k_\beta\boldsymbol{\beta}+k_\gamma\boldsymbol{\gamma})=\epsilon_n(-k_\alpha\boldsymbol{\alpha}+\tilde{\kappa}_\beta\boldsymbol{\beta}+\tilde{\kappa}_\gamma\boldsymbol{\gamma})$—the band dispersion $\epsilon_n(\mathbf{k})$ being symmetric with respect to k_α. This implies that $\partial\epsilon_n(\mathbf{k})/\partial k_\alpha$ at $\mathbf{k}$ and $\mathbf{k}'$ are opposite numbers, while the other two quantities [i.e., $\partial^2\epsilon_n(\mathbf{k})/\partial k_\alpha^2$ and $df_0(\epsilon_n)/d\epsilon_n$] are identical. Associated with each ϵ_n, the integral function in Eq. (1) cancels out over the integration region, and this yields null $J_\alpha^{(2)}$. To achieve nonzero $J_\alpha^{(2)}$, the linkage between k_α and $-k_\alpha$ must be broken, namely, $\epsilon_n(k_\alpha\boldsymbol{\alpha}+k_\beta\boldsymbol{\beta}+k_\gamma\boldsymbol{\gamma})$ is never symmetrically related to $\epsilon_n(-k_\alpha\boldsymbol{\alpha}+\tilde{\kappa}_\beta\boldsymbol{\beta}+\tilde{\kappa}_\gamma\boldsymbol{\gamma})$ no matter what $\tilde{\kappa}_\beta$ and $\tilde{\kappa}_\gamma$ are selected. In view of this, $J_\alpha^{(2)}$ only occurs in materials with specific symmetry constraints. For example, materials with time-reversal symmetry $\mathbb{1}'$ do not host $J_\alpha^{(2)}$, because $\mathbb{1}'$ links $k_\alpha\boldsymbol{\alpha}+k_\beta\boldsymbol{\beta}+k_\gamma\boldsymbol{\gamma}$ with $-k_\alpha\boldsymbol{\alpha}-k_\beta\boldsymbol{\beta}-k_\gamma\boldsymbol{\gamma}$. On the contrary, materials with magnetic order parameter L (i.e., broken time-reversal symmetry) might be compatible with $J_\alpha^{(2)}$ [55]. As analyzed in Sec. I of the Supplemental Material [26], $J_\alpha^{(2)}$ is a function of L, and the nonlinear longitudinal Drude conductivity $\sigma_{\alpha\alpha\alpha}^{(2)}$ is given by

$$\sigma_{\alpha\alpha\alpha}^{(2)}=\frac{\zeta(L)e^3\tau^2}{8\pi^3\hbar^3}\sum_n\iiint\frac{\partial^2\epsilon_n}{\partial k_\alpha^2}\frac{df_0(\epsilon_n)}{d\epsilon_n}\frac{\partial\epsilon_n}{\partial k_\alpha}d^3\mathbf{k},\qquad(2)$$

where $\zeta(L)=\pm1$ and $\zeta(-L)=-\zeta(L)$ indicate the dependence of $\sigma_{\alpha\alpha\alpha}^{(2)}$ on L [56]. We now show that $\sigma_{\alpha\alpha\alpha}^{(2)}$ contributes to longitudinal NCT, by examining the current density $J_\alpha=\sigma_{\alpha\alpha}^{(1)}E_\alpha+\sigma_{\alpha\alpha\alpha}^{(2)}E_\alpha^2$ [11,23], with $\sigma_{\alpha\alpha}^{(1)}$ being the linear conductivity; In first approximation, the electric field is expressed as $E_\alpha\approx J_\alpha/\sigma_{\alpha\alpha}^{(1)}$. This suggests that $J_\alpha/E_\alpha=\sigma_{\alpha\alpha}^{(1)}+\sigma_{\alpha\alpha\alpha}^{(2)}E_\alpha\approx\sigma_{\alpha\alpha}^{(1)}+\sigma_{\alpha\alpha\alpha}^{(2)}J_\alpha/\sigma_{\alpha\alpha}^{(1)}\equiv\sigma_{\alpha\alpha}^{(1)}+\xi_\alpha J_\alpha\zeta(L)$ (ξ_α being a coefficient). The term $\xi_\alpha J_\alpha\zeta(L)$ resembles $R(B)=\xi BI$ as follows: reversing L or J_α changes the sign of $\sigma_{\alpha\alpha\alpha}^{(2)}$, where L and J_α play the roles as B and I, respectively. In other words, the nonlinear conductivity $\sigma_{\alpha\alpha\alpha}^{(2)}$ characterizes the longitudinal NCT along α direction.

Symmetry analysis—We move on to carry out symmetry analysis regarding the longitudinal NCT. We use the $m'm2'$ magnetic point group (MPG) to demonstrate our basic ideas. This MPG contains four symmetry operations, namely, $\mathbb{1}$, $\mathfrak{m}_y$, $\mathfrak{m}_x'$, and $\mathbb{2}_z'$. The $\mathbb{1}$ symmetry operation is the identity, and has no effect on $(k_x,k_y,k_z)\equiv k_x\mathbf{x}+k_y\mathbf{y}+k_z\mathbf{z}$ ($\mathbf{x}$, $\mathbf{y}$, $\mathbf{z}$ being unit vectors along the Cartesian x, y, z directions). The $\mathfrak{m}_y$ operation is a mirror plane perpendicular to y, and it transforms (k_x,k_y,k_z) to $(k_x,-k_y,k_z)$. The $\mathfrak{m}_x'$ operation, the mirror plane perpendicular to x followed by a time-reversal operation, transforms (k_x,k_y,k_z) to $(k_x,-k_y,-k_z)$. Finally, (k_x,k_y,k_z) is transformed to $(k_x,k_y,-k_z)$ by $\mathbb{2}_z'$, the twofold rotation along z followed by a time reversal. On balance, the symmetry operations of the $m'm2'$ MPG (i) link k_y with $-k_y$ by $\mathfrak{m}_y$ or $\mathfrak{m}_x'$, (ii) link k_z with $-k_z$ by $\mathfrak{m}_x'$ or $\mathbb{2}_z'$, and (iii) provide no linkage between k_x and $-k_x$. This means that the longitudinal NCT in $m'm2'$ MPG is symmetrically allowed along the x direction.

TABLE I. The 42 MPGs that allow the longitudinal NCT. For each MPG, the ✓ and ✗ indicate that longitudinal NCT along the α direction is symmetrically allowed and forbidden, respectively. Here, $\alpha = x, y, z$ marks the direction in the Cartesian frame. The conventions regarding the coordinate system for these MPGs are shown in Table S1 of the Supplemental Material [26].

MPGs	x	y	z	MPGs	x	y	z	MPGs	x	y	z
1.1	✓	✓	✓	$\bar{1}'$	✓	✓	✓	2.1	✗	✗	✓
$2'$	✓	✓	✗	$m.1$	✓	✓	✗	m'	✗	✗	✓
$2'/m$	✓	✓	✗	$2/m'$	✗	✗	✓	$2'2'2$	✗	✗	✓
$mm2.1$	✗	✗	✓	$m'm2'$	✓	✗	✗	$m'mm$	✓	✗	✗
4.1	✗	✗	✓	$\bar{4}'$	✗	✗	✓	$4/m'$	✗	✗	✓
$42'2'$	✗	✗	✓	$4mm.1$	✗	✗	✓	$\bar{4}'2'm$	✗	✗	✓
$4/m'mm$	✗	✗	✓	3.1	✓	✓	✓	$\bar{3}'$	✓	✓	✓
32.1	✓	✗	✗	$32'$	✗	✓	✓	$3m.1$	✗	✓	✓
$3m'$	✓	✗	✗	$\bar{3}'m$	✗	✓	✓	$\bar{3}'m'$	✓	✗	✗
6.1	✗	✗	✓	$6'$	✓	✓	✗	$\bar{6}.1$	✓	✓	✗
$\bar{6}'$	✗	✗	✓	$6'/m$	✓	✓	✗	$6/m'$	✗	✗	✓
$6'22'$	✓	✗	✗	$62'2'$	✗	✗	✓	$6mm.1$	✗	✗	✓
$6'mm'$	✗	✓	✗	$\bar{6}m2.1$	✗	✓	✗	$\bar{6}'m2'$	✗	✗	✓
$\bar{6}m'2'$	✓	✗	✗	$6/m'mm$	✗	✗	✓	$6'/mmm'$	✗	✓	✗

TABLE II. The magnetic field induced longitudinal NCT in 20 type-2 MPGs. The B_x, B_y, and B_z mark the x, y, and z components of the magnetic field, respectively. The directions for longitudinal NCT are labeled by x, y, and z (Cartesian frame). The conventions regarding the coordinate system for these MPGs are shown in Table S1 of the Supplemental Material [26].

MPGs	B_x	B_y	B_z	MPGs	B_x	B_y	B_z
$1.1'$	x, y, z	x, y, z	x, y, z	$2.1'$	x, y	x, y	z
$m.1'$	z	z	x, y	$222.1'$	x	y	z
$mm2.1'$	y	x	$\cdots$	$4.1'$	x, y	x, y	z
$\bar{4}.1'$	x, y	x, y	$\cdots$	$422.1'$	x	y	z
$4mm.1'$	y	x	$\cdots$	$\bar{4}2m.1'$	x	y	$\cdots$
$3.1'$	x, y, z	x, y, z	x, y, z	$32.1'$	x	y, z	y, z
$3m.1'$	y, z	x	x	$6.1'$	x, y	x, y	z
$\bar{6}.1'$	z	z	x, y	$622.1'$	x	y	z
$6mm.1'$	y	x	$\cdots$	$\bar{6}m2.1'$	z	$\cdots$	x
$23.1'$	x	y	z	$432.1'$	x	y	z

In this way, we conduct symmetry analysis on the complete 122 MPGs (see Sec. II of the Supplemental Material [26] for details). These groups are composed of 32 type-1 MPGs, 32 type-2 MPGs, and 58 type-3 MPGs [57,58], where type-2 MPGs contain time-reversal symmetry $1'$, but type-1 and type-3 MPGs do not have $1'$ [59]. Among type-1 and type-3 MPGs, 42 cases host symmetrically allowed longitudinal NCT (see Table I). As for type-2 MPGs, the time-reversal symmetry therein forbids longitudinal NCT; Nonetheless, magnetic field breaks time-reversal and other symmetries in type-2 MPGs, possibly yielding longitudinal NCT. Regarding this, we analyze the magnetic field induced symmetry breakings in type-2 MPGs, and identify 20 cases in which magnetic field enables longitudinal NCT (see Table II) [60].

Tables I and II, obtained with respect to nonlinear Drude conductivity $\sigma^{(2)}_{\alpha\alpha\alpha} \propto \tau^2$, are also valid for quantum metric contributed conductivity $\tilde{\sigma}^{(2)}_{\alpha\alpha\alpha} \propto \tau^0$, since $\tilde{\sigma}^{(2)}_{\alpha\alpha\alpha}$ is rooted in the asymmetry between k_α and $-k_\alpha$ as well [14,15]. That is, an MPG allowing $\sigma^{(2)}_{\alpha\alpha\alpha}$ naturally enables $\tilde{\sigma}^{(2)}_{\alpha\alpha\alpha}$ (vice versa), and the measured longitudinal NCT along α direction should be a mixture of $\sigma^{(2)}_{\alpha\alpha\alpha}$ and $\tilde{\sigma}^{(2)}_{\alpha\alpha\alpha}$. Depending on materials, nonreciprocal conductivity from nonlinear Drude may be primary or secondary compared with that from quantum metric. For instance, nonreciprocal conductivities in two-layer-thick $MnBi_2Te_4$ are mainly contributed by nonlinear Drude, while those in four-layer-thick $MnBi_2Te_4$ are mostly from quantum metric [15]. Moreover, nonlinear Drude conductivity ($\propto \tau^2$) can be significantly enhanced by improving carrier relaxation time τ (via, e.g., the optimization of carrier concentration [61]).

Effective Hamiltonians for longitudinal NCT—In this section, we explore the role of magnetic order parameter L in band asymmetry and longitudinal NCT. For this purpose, we derive the minimal two-band effective Hamiltonians for the 42 MPGs listed in Table I, involving the magnetic order parameter L, the wave vector $\mathbf{k}$, and the electronic spin $\boldsymbol{\sigma} \equiv (\sigma_x, \sigma_y, \sigma_z)$—$\boldsymbol{\sigma}$ being Pauli matrix vector. The results are summarized in Tables S3 and S4 of the Supplemental Material [26]. The effective Hamiltonians (around the center of the Brillouin zone) for these 42 MPGs are generally written as

$$H(\mathbf{k}, L) = \sum_{\alpha,\beta=x,y,z} \mu_{\alpha\beta} k_\alpha k_\beta \sigma_0 + \zeta(L)\Lambda(\mathbf{k})\sigma_0 + \boldsymbol{\lambda}(\mathbf{k}) \cdot \boldsymbol{\sigma} + \zeta(L)\boldsymbol{\Delta} \cdot \boldsymbol{\sigma}, \tag{3}$$

where $\mu_{\alpha\beta}$, $\Lambda(\mathbf{k})$, $\boldsymbol{\lambda}(\mathbf{k})$, and $\boldsymbol{\Delta}$ characterize the effective mass, band asymmetry, spin-orbit field, and Zeeman field, respectively (σ_0 being 2×2 identity matrix). The effective mass terms and band asymmetry terms appear in the effective Hamiltonians of all these 42 MPGs. Furthermore, MPGs lacking the parity-time symmetry (i.e., inversion followed by time reversal) may also have spin-orbit field terms, while MPGs compatible with ferromagnetism extra gain Zeeman field terms. Of particular interest is the $\zeta(L)\Lambda(\mathbf{k})\sigma_0$ band asymmetry term, with $\Lambda(\mathbf{k})$ being an odd function of k_χ. Such a term describes the band asymmetry with respect to k_χ as well as the longitudinal NCT along the χ direction. As for the spin-orbit field and Zeeman field terms, the situation becomes quite complicated. This will be discussed in the following paragraphs.

We now take a few representative MPGs to perform our Hamiltonian analysis. Our first example is the $6mm.1$ MPG with its effective Hamiltonian given by $H_1(\mathbf{k}, L) = \mu_{xx}(k_x^2 + k_y^2)\sigma_0 + \mu_{zz}k_z^2\sigma_0 + \zeta(L)\Lambda_z k_z \sigma_0 + \lambda_{xy}(k_x\sigma_y - k_y\sigma_x)$.

This Hamiltonian contains the effective mass terms, the band asymmetry term, and the spin-orbit field terms (no Zeeman field terms). Some other MPGs may have effective Hamiltonians with only effective mass terms and band asymmetry terms. For instance, the effective Hamiltonians for $4/m'mm$ and $6'/mmm'$ MPGs are $H_2(\mathbf{k}, L) = \mu_{xx}(k_x^2 + k_y^2)\sigma_0 + \mu_{zz}k_z^2\sigma_0 + \zeta(L)\Lambda_z k_z \sigma_0$ and $H_3(\mathbf{k}, L) = \mu_{xx}(k_x^2 + k_y^2)\sigma_0 + \mu_{zz}k_z^2\sigma_0 + \zeta(L)\Lambda_{yyy}k_y(3k_x^2 - k_y^2)\sigma_0$, respectively. The role of L on the band asymmetry and longitudinal NCT can be illustrated by numerically solving $H_2(\mathbf{k}, L)$ and $H_3(\mathbf{k}, L)$, with various groups of selected model parameters. As shown in Fig. 1(a), the nonzero $\zeta(L)\Lambda_z$ results in band asymmetry along the k_z direction, where the $-L$ and $+L$ magnetic order parameters yield two versions of bands (red and blue lines) being mirror copies of each other with respect to $k_z = 0$. This is responsible for the longitudinal nonreciprocal $\sigma_{zzz}^{(2)}$ electric conductivity, whose sign is reversed by switching magnetic order parameters between L and $-L$ [Fig. 1(b)]. When removing the magnetic order parameter L [i.e., $\zeta(L) = 0$], both the band asymmetry and longitudinal $\sigma_{zzz}^{(2)}$ conductivity vanish [see Figs. 1(a) and 1(b)]. As for $H_3(\mathbf{k}, L)$, the $\zeta(L)\Lambda_{yyy}k_y(3k_x^2 - k_y^2)\sigma_0$ term is cubic in k_y, which yields the band asymmetry and longitudinal NCT along y [see Figs. 1(c) and 1(d)]. Various MPGs (e.g., $\bar{1}'$, $m'mm$, and $\bar{3}'$) have effective Hamiltonians similar to $H_1(\mathbf{k}, L)$, $H_2(\mathbf{k}, L)$, or $H_3(\mathbf{k}, L)$, that is, with band asymmetry terms and without Zeeman field terms. In such Hamiltonians, the longitudinal NCT is solely governed by the band asymmetry terms, which is spin independent.

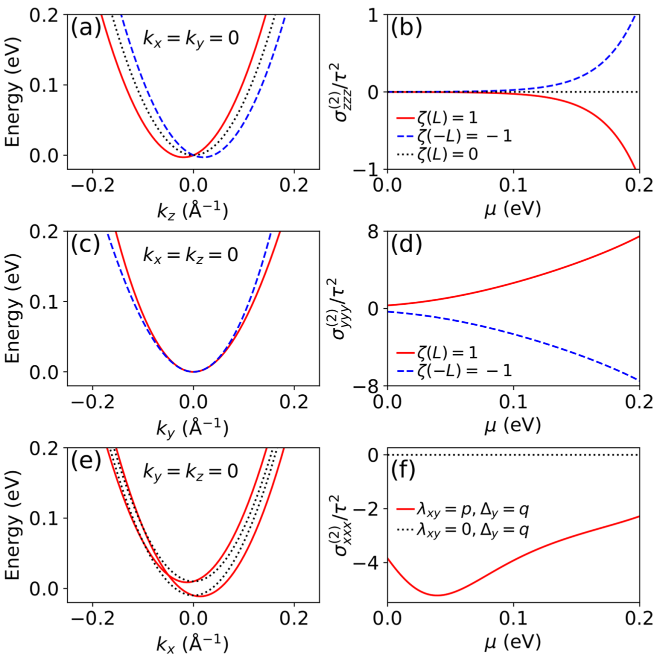

FIG. 1. Band structures and longitudinal NCT obtained from various Hamiltonians. (a) and (b): $H_2(\mathbf{k}, L) = \mu_{xx}(k_x^2 + k_y^2)\sigma_0 + \mu_{zz}k_z^2\sigma_0 + \zeta(L)\Lambda_z k_z\sigma_0$ with $\Lambda_z = 0.3$ eV Å. (c) and (d): $H_3(\mathbf{k}, L) = \mu_{xx}(k_x^2 + k_y^2)\sigma_0 + \mu_{zz}k_z^2\sigma_0 + \zeta(L)\Lambda_{yyy}k_y(3k_x^2 - k_y^2)\sigma_0$ with $\Lambda_{yyy} = 5.0$ eV Å^3. (e) and (f): $H_4(\mathbf{k}, L) = (\mu_{xx}k_x^2 + \mu_{yy}k_y^2 + \mu_{zz}k_z^2)\sigma_0 + \zeta(L)\Lambda_x k_x\sigma_0 + \zeta(L)\Delta_y\sigma_y + \lambda_{xy}k_x\sigma_y + \lambda_{yx}k_y\sigma_x$, with $\Lambda_x = 0.0$ eV Å, $\lambda_{yx} = 0.3$ eV Å, $p = 0.2$ eV Å, $q = 0.01$ eV, and $\zeta(L) = 1$. $\zeta(L) = 1$ and $\zeta(-L) = -1$ corresponds to L and $-L$, respectively. As for $H_2(\mathbf{k}, L)$, $H_3(\mathbf{k}, L)$, and $H_4(\mathbf{k}, L)$, μ_{xx}, μ_{yy}, and μ_{zz} are set as $\mu_{xx} = \mu_{yy} = \mu_{zz} = \hbar^2/2m = 7.62$ eV Å^2, where $m = 0.5m_0$ and m_0 is electron rest mass. The unit of $\sigma_{zzz}^{(2)}/\tau^2$, $\sigma_{yyy}^{(2)}/\tau^2$, and $\sigma_{xxx}^{(2)}/\tau^2$ is $10^{23}\ \Omega^{-1}\,\mathrm{V}^{-1}\,\mathrm{s}^{-2}$. The thermal smearing with a temperature of 300 K is adopted during the conductivity calculations. The legends for (b), (d), and (f) are valid for (a), (c), and (e), respectively. Note that the band minimum associated with the red or blue curve in (a), (b), (e), and (f) is below $\mu = 0$ eV.

The $m'm2'$ is another exemplified MPG with an effective Hamiltonian $H_4(\mathbf{k}, L) = (\mu_{xx}k_x^2 + \mu_{yy}k_y^2 + \mu_{zz}k_z^2)\sigma_0 + \zeta(L)\Lambda_x k_x\sigma_0 + \zeta(L)\Delta_y\sigma_y + \lambda_{xy}k_x\sigma_y + \lambda_{yx}k_y\sigma_x$. Such a Hamiltonian contains the effective mass terms, the spin-orbit field terms, a band asymmetry term, and a Zeeman field term. Regarding $H_4(\mathbf{k}, L)$, there are two mechanisms responsible for the longitudinal NCT. First of all, the $\zeta(L)\Lambda_x k_x\sigma_0$ term suggests a longitudinal NCT along the x direction. This mechanism has already been discussed in the last paragraph. The second mechanism comes from the combination of spin-orbit field term $\lambda_{xy}k_x\sigma_y$ and Zeeman field term $\zeta(L)\Delta_y\sigma_y$, which gives rise to band asymmetry along k_x and longitudinal $\sigma_{xxx}^{(2)}$ conductivity [see Figs. 1(e) and 1(f)]. This situation likely occurs when the spin-orbit field and Zeeman field cooperatively break the symmetric linkage between k_x and $-k_x$. Without $\lambda_{xy}k_x\sigma_y$ or $\zeta(L)\Lambda_x k_x\sigma_0$, $\zeta(L)\Delta_y\sigma_y$ cannot solely generate band asymmetry or longitudinal NCT [see Figs. 1(e) and 1(f)]. Previous studies usually consider spin-orbit field terms and Zeeman field terms, but neglecting the $\zeta(L)\Lambda(\mathbf{k})\sigma_0$ term (see, e.g., Refs. [5,6,9,23,62]). Even though the combination of $\zeta(L)\Delta_\alpha\sigma_\alpha$ and $\lambda_\alpha(\mathbf{k})\sigma_\alpha$ might capture the longitudinal NCT, there are no reasons to ignore $\zeta(L)\Lambda(\mathbf{k})\sigma_0$.

For type-2 MPGs (Table II), the effective Hamiltonians are generally $H(\mathbf{k}) = \sum_{\alpha,\beta}\mu_{\alpha\beta}k_\alpha k_\beta\sigma_0 + \boldsymbol{\lambda}(\mathbf{k})\cdot\boldsymbol{\sigma}$, where time-reversal $\imath'$ forbids band asymmetry and Zeeman field terms. The $\boldsymbol{\lambda}(\mathbf{k})\cdot\boldsymbol{\sigma}$ in $H(\mathbf{k})$ may contain a nonzero $\lambda_\beta(k_\alpha)\sigma_\beta$ term, with $\lambda_\beta(k_\alpha)$ being an odd function of k_α [54]. In this situation, applying magnetic field B_γ creates $\Delta_\beta(B_\gamma)\sigma_\beta$ and $\Lambda_{\beta\gamma\alpha}\Delta_\beta(B_\gamma)\lambda_\beta(k_\alpha)\sigma_0$ couplings, where $\Delta_\beta(B_\gamma)$ is an odd function of B_γ. This yields the longitudinal NCT along the α direction.

The longitudinal NCT in ε-Fe_2O_3—Tables I and II guide the discovery of materials with longitudinal NCT. We are motivated by the design of intrinsic semiconductor diodes, and decide to seek semiconductors with longitudinal NCT. Searching from the MAGNDATA database [63], we identify multiferroic ε-Fe_2O_3 as a promising candidate. ε-Fe_2O_3

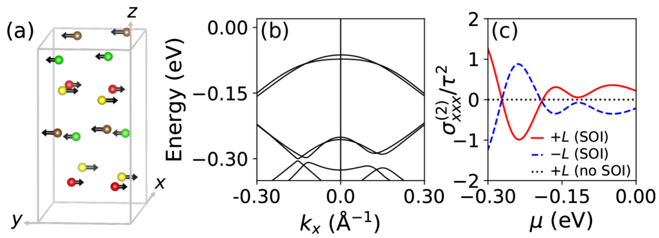

FIG. 2. The $+L$ magnetic order parameter (a), band dispersion (b), and nonlinear Drude conductivity (c) of ε-Fe_2O_3. In (a), brown, yellow, red, and green spheres denote Fe1, Fe2, Fe3, and Fe4 sublattices (O ions not shown), respectively. The arrows represent the predominant components of Fe's magnetic moments. In (b), the band dispersion is along k_x, where k_y and k_z are set to zero. The valence band maximum is set as the zero energy. In (c), $-L$ corresponds to the reversed $+L$ magnetic order parameter; "SOI" and "no SOI" indicate that the calculations are done with and without spin-orbit interaction, respectively. The unit of $\sigma^{(2)}_{xxx}/\tau^2$ is $10^{23}\ \Omega^{-1}\ \mathrm{V}^{-1}\ \mathrm{s}^{-2}$.

is the metastable phase of Fe_2O_3 [64–67]. Recently, single crystals of ε-Fe_2O_3 were experimentally synthesized [66]. At room temperature, ε-Fe_2O_3 has the polar $m'm2'$ MPG, with the magnetic order parameter schematized in Fig. 2(a) [63–65]. According to Table I, the longitudinal NCT along the x direction is symmetrically allowed in ε-Fe_2O_3.

Figure 2(b) demonstrates ε-Fe_2O_3's band asymmetry along k_x. In Fig. 2(c), we show the nonlinear Drude conductivity $\sigma^{(2)}_{xxx}$ for ε-Fe_2O_3 [68]. We find that $\sigma^{(2)}_{xxx}$ is negligible in the absence of spin-orbit interaction. The role of spin-orbit interaction for $\sigma^{(2)}_{xxx}$ is thus self-explanatory. With spin-orbit interaction, the nonlinear Drude conductivity $\sigma^{(2)}_{xxx}$ becomes finite, and is reversible by flipping the magnetic order parameter L. This verifies our aforementioned symmetry arguments on ε-Fe_2O_3. Our calculations, although based on the ground state of ε-Fe_2O_3, correctly reflect the MPG of such a material at room temperature. This suggests that ε-Fe_2O_3 may host room-temperature longitudinal NCT that is driven by its intrinsic magnetic order parameter (i.e., without the application of external magnetic field).

As shown in the *symmetry analysis* section, the longitudinal NCT in ε-Fe_2O_3 is contributed by nonlinear Drude conductivity $\sigma^{(2)}_{xxx}$ and quantum metric conductivity $\tilde{\sigma}^{(2)}_{xxx}$. At 300 K, we estimate ε-Fe_2O_3's $\sigma^{(2)}_{xxx}$ as several tenths of $\mathrm{mA/V^2}$ by selecting a typical relaxation time of $\tau = 60$ fs [61]. Decreasing temperature or improving relaxation time may enhance $\sigma^{(2)}_{xxx}$. Furthermore, $\sigma^{(2)}_{xxx}$ conductivity is distinguishable from $\tilde{\sigma}^{(2)}_{xxx}$ due to their different scaling behaviors with respect to τ [14,15]. The detailed discussion is shown in Sec. V of the Supplemental Material [26].

Summary and perspective—In summary, we have developed a general theory guiding the discovery of crystalline materials with longitudinal NCT. Within the framework of Boltzmann transport theory, the longitudinal NCT along α direction in crystalline materials resides in the asymmetry between k_α and $-k_\alpha$. Based on this, we provide a comprehensive symmetry classification of 122 MPGs with respect to longitudinal NCT (see Tables I and II). By constructing and analyzing effective Hamiltonians, we identify two mechanisms for longitudinal NCT, that is, the band asymmetry $\Lambda(\mathbf{k})$, and the combination of spin-orbit field $\boldsymbol{\lambda}(\mathbf{k})$ and Zeeman field $\boldsymbol{\Delta}$ [see Eq. (3)]. Our theory, together with first-principles simulations help to identify ε-Fe_2O_3 as a candidate that possibly showcases intrinsic longitudinal NCT at room temperature.

Beyond this, our theory also suggests another research avenue. As shown in Figs. 1 and 2, the longitudinal NCT severely depends on the magnetic order parameters. For a specific material with MPG listed in Tables I and II, the measurement of nonlinear longitudinal conductivity reflects its intrinsic magnetic ordering or the external magnetic field applied to it. In this regard, the longitudinal NCT together with second-order transverse Drude transport and second-order anomalous Hall effect (i.e., second-order nonlinear transport) open a door for the electrical detection of magnetic states [10,69,70], being important for designing spintronic devices [71–74]. Interested readers are referred to Refs. [15,69,70,75] for some detailed discussion on second-order nonlinear transport. As an outlook, our theory can not only provide in-depth insights into the NCT phenomena in condensed matter, but also guide the materials discovery and device design related to such a phenomenon.

Acknowledgments—We acknowledge the support from the National Natural Science Foundation of China (Grants No. 12274174, No. 12274102, No. 22090044, No. 52288102, No. 52090024, and No. 12034009), the National Key Research and Development Program of China (Grant No. 2022YFA1402501), the Strategic Priority Research Program of Chinese Academy of Sciences (Grant No. XDB33000000), and the Fundamental Research Funds for the Central Universities (Grant No. FRFCU5710053421, No. HIT.OCEF.2023031). L. B. thanks the Vannevar Bush Faculty Fellowship (VBFF) Grant No. N00014-20-1-2834 from the Department of Defense and Grant No. DMR-1906383 from the National Science Foundation AMASE-i Program (MonArk NSF Quantum Foundry). H. J. Z. thanks the "Xiaomi YoungScholar" Project.

[1] R. Wakatsuki, Y. Saito, S. Hoshino, Y. M. Itahashi, T. Ideue, M. Ezawa, Y. Iwasa, and N. Nagaosa, Sci. Adv. **3**, e1602390 (2017).
[2] M. Nadeem, M. S. Fuhrer, and X. Wang, Nat. Rev. Phys. **5**, 558 (2023).
[3] Y. Tokura and N. Nagaosa, Nat. Commun. **9**, 3740 (2018).
[4] S. N. Makarov, R. Ludwig, and S. J. Bitar, Electronic diode and diode circuits, in *Practical Electrical Engineering*

(Springer International Publishing, New York, 2016), pp. 795–849, 10.1007/978-3-319-21173-2_16.
[5] T. Ideue, K. Hamamoto, S. Koshikawa, M. Ezawa, S. Shimizu, Y. Kaneko, Y. Tokura, N. Nagaosa, and Y. Iwasa, Nat. Phys. **13**, 578 (2017).
[6] Y. Li, Y. Li, P. Li, B. Fang, X. Yang, Y. Wen, D.-x. Zheng, C.-h. Zhang, X. He, A. Manchon, Z.-H. Cheng, and X.-x. Zhang, Nat. Commun. **12**, 540 (2021).
[7] M. Suárez-Rodríguez, B. Martín-García, W. Skowroński, F. Calavalle, S. S. Tsirkin, I. Souza, F. De Juan, A. Chuvilin, A. Fert, M. Gobbi, F. Casanova, and L. E. Hueso, Phys. Rev. Lett. **132**, 046303 (2024).
[8] M. Kocsis, O. Zheliuk, P. Makk, E. Tóvári, P. Kun, O. E. Tereshchenko, K. A. Kokh, T. Taniguchi, K. Watanabe, J. Ye, and S. Csonka, Phys. Rev. Res. **3**, 033253 (2021).
[9] R. Yoshimi, M. Kawamura, K. Yasuda, A. Tsukazaki, K. S. Takahashi, M. Kawasaki, and Y. Tokura, Phys. Rev. B **106**, 115202 (2022).
[10] W. Chen, M. Gu, J. Li, P. Wang, and Q. Liu, Phys. Rev. Lett. **129**, 276601 (2022).
[11] J. Železný, Z. Fang, K. Olejník, J. Patchett, F. Gerhard, C. Gould, L. W. Molenkamp, C. Gomez-Olivella, J. Zemen, T. Tichý, T. Jungwirth, and C. Ciccarelli, Phys. Rev. B **104**, 054429 (2021).
[12] Y. Wang, H. F. Legg, T. Bömerich, J. Park, S. Biesenkamp, A. A. Taskin, M. Braden, A. Rosch, and Y. Ando, Phys. Rev. Lett. **128**, 176602 (2022).
[13] Z. Zhang, N. Wang, N. Cao, A. Wang, X. Zhou, K. Watanabe, T. Taniguchi, B. Yan, and W.-b. Gao, Nat. Commun. **13**, 6191 (2022).
[14] N. Wang, D. Kaplan, Z. Zhang, T. Holder, N. Cao, A. Wang, X. Zhou, F. Zhou, Z. Jiang, C. Zhang, S. Ru, H. Cai, K. Watanabe, T. Taniguchi, B. Yan, and W. Gao, Nature (London) **621**, 487 (2023).
[15] D. Kaplan, T. Holder, and B. Yan, Phys. Rev. Lett. **132**, 026301 (2024).
[16] D. Szaller, S. Bordács, and I. Kézsmárki, Phys. Rev. B **87**, 014421 (2013).
[17] Z. Z. Du, H.-Z. Lu, and X. C. Xie, Nat. Rev. Phys. **3**, 744 (2021).
[18] G. L. J. A. Rikken, J. Fölling, and P. Wyder, Phys. Rev. Lett. **87**, 236602 (2001).
[19] G. L. J. A. Rikken and P. Wyder, Phys. Rev. Lett. **94**, 016601 (2005).
[20] T. Guillet, C. Zucchetti, Q. Barbedienne, A. Marty, G. Isella, L. Cagnon, C. Vergnaud, H. Jaffrès, N. Reyren, J.-M. George, A. Fert, and M. Jamet, Phys. Rev. Lett. **124**, 027201 (2020).
[21] Our theory focuses on longitudinal NCT in response to direct electric field or alternating electric field with ultralow frequencies (e.g., < 1000 Hz). The discussion on nonlinear optical phenomena is therefore excluded, since such phenomena respond to oscillating fields with optical frequencies (i.e., $\sim 10^{14}$ Hz) [17].
[22] R. Wakatsuki and N. Nagaosa, Phys. Rev. Lett. **121**, 026601 (2018).
[23] S. Hoshino, R. Wakatsuki, K. Hamamoto, and N. Nagaosa, Phys. Rev. B **98**, 054510 (2018).
[24] H. Isobe, S.-Y. Xu, and L. Fu, Sci. Adv. **6**, eaay2497 (2020).
[25] I. Sodemann and L. Fu, Phys. Rev. Lett. **115**, 216806 (2015).
[26] See Supplemental Material at http://link.aps.org/supplemental/10.1103/PhysRevLett.133.096802 for the derivations and symmetry analysis on longitudinal NCT, the derivations of effective Hamiltonians, the methods, and the supplementary discussion on the experimental probe of longitudinal NCT.
[27] K. Hamamoto, M. Ezawa, K. W. Kim, T. Morimoto, and N. Nagaosa, Phys. Rev. B **95**, 224430 (2017).
[28] Mpoint, https://www.cryst.ehu.es/cryst/mpoint.html.
[29] M. S. Dresselhaus, G. Dresselhaus, and A. Jorio, *Group Theory: Application to the Physics of Condensed Matter* (Springer Berlin Heidelberg, Berlin, Heidelberg, 2008).
[30] Mgenpos, https://www.cryst.ehu.es/cgi-bin/cryst/programs/magget_gen.pl.
[31] L.-D. Yuan, Z. Wang, J.-W. Luo, and A. Zunger, Phys. Rev. Mater. **5**, 014409 (2021).
[32] L. C. L. Y. Voon and M. Willatzen, *The k·p Method: Electronic Properties of Semiconductors* (Springer Berlin Heidelberg, Berlin, Heidelberg, 2009).
[33] R. Winkler and U. Zülicke, Phys. Rev. B **82**, 245313 (2010).
[34] R. Winkler, *Spin-Orbit Coupling Effects in Two-Dimensional Electron and Hole Systems* (Springer Berlin Heidelberg, Berlin, Heidelberg, 2003).
[35] G. Kresse and J. Furthmüller, Phys. Rev. B **54**, 11169 (1996).
[36] G. Kresse and D. Joubert, Phys. Rev. B **59**, 1758 (1999).
[37] P. E. Blöchl, Phys. Rev. B **50**, 17953 (1994).
[38] D. M. Ceperley and B. J. Alder, Phys. Rev. Lett. **45**, 566 (1980).
[39] S. L. Dudarev, G. A. Botton, S. Y. Savrasov, C. J. Humphreys, and A. P. Sutton, Phys. Rev. B **57**, 1505 (1998).
[40] G. K. Madsen, J. Carrete, and M. J. Verstraete, Comput. Phys. Commun. **231**, 140 (2018).
[41] Y. Jin, X. Wang, M. Yao, D. Qiu, D. J. Singh, J. Xi, J. Yang, and L. Xi, npj Comput. Mater. **9**, 190 (2023).
[42] K. Momma and F. Izumi, J. Appl. Crystallogr. **44**, 1272 (2011).
[43] J. D. Hunter, Comput. Sci. Eng. **9**, 90 (2007).
[44] H. T. Stokes, D. M. Hatch, and B. J. Campbell, FINDSYM, ISOTROPY Software Suite, https://iso.byu.edu.
[45] H. T. Stokes and D. M. Hatch, J. Appl. Crystallogr. **38**, 237 (2005).
[46] M. I. Aroyo, A. Kirov, C. Capillas, J. M. Perez-Mato, and H. Wondratschek, Acta Crystallogr. Sect. A **62**, 115 (2006).
[47] M. I. Aroyo, J. M. Perez-Mato, C. Capillas, E. Kroumova, S. Ivantchev, G. Madariaga, A. Kirov, and H. Wondratschek, Z. Kristallogr. Cryst. Mater. **221**, 15 (2006).
[48] M. I. Aroyo, J. M. Perez-Mato, D. Orobengoa, E. Tasci, G. de la Flor, and A. Kirov, Bulg. Chem. Commun. **43**, 183 (2011).
[49] S. V. Gallego, J. M. Perez-Mato, L. Elcoro, E. S. Tasci, R. M. Hanson, K. Momma, M. I. Aroyo, and G. Madariaga, J. Appl. Crystallogr. **49**, 1750 (2016).
[50] S. V. Gallego, J. M. Perez-Mato, L. Elcoro, E. S. Tasci, R. M. Hanson, M. I. Aroyo, and G. Madariaga, J. Appl. Crystallogr. **49**, 1941 (2016).

[51] J. M. Ziman, *Principles of the Theory of Solids* (Cambridge University Press, Cambridge, England, 1972).

[52] Z. Dauter and M. Jaskolski, J. Appl. Crystallogr. **43**, 1150 (2010).

[53] X. Liu, H. J. Zhao, L. Bellaiche, and Y. Ma, Phys. Rev. B **108**, 125108 (2023).

[54] H. J. Zhao, H. Nakamura, R. Arras, C. Paillard, P. Chen, J. Gosteau, X. Li, Y. Yang, and L. Bellaiche, Phys. Rev. Lett. **125**, 216405 (2020).

[55] The word "might" means that the broken time-reversal symmetry is not the sufficient condition for the nonreciprocal charge transport. As a matter of fact, the other symmetry operations (e.g., spatial inversion) also constrain the behaviors of nonreciprocal charge transport. This will be demonstrated in the following section.

[56] In materials with magnetic order parameter L, the first-order linear charge current remains invariant when reversing L (e.g., from L to $-L$). The detailed analysis can be found in Sec. I of the Supplemental Material [26].

[57] B. J. Campbell, H. T. Stokes, J. M. Perez-Mato, and J. Rodríguez-Carvajal, Acta Crystallogr. Sect. A **78**, 99 (2022).

[58] M. El-Batanouny and F. Wooten, *Symmetry and Condensed Matter Physics: A Computational Approach* (Cambridge University Press, Cambridge, England, 2008).

[59] The difference between type-1 and type-3 MPGs is that the former contain only the spatial symmetry operations, while the latter also involve some symmetry operations being a spatial operation followed by $1'$ (see, e.g., Ref. [57] for details).

[60] In first approximation, complex magnetic field away from x, y, or z orientation can be seen as a superposition of two or three components among B_x, B_y, and B_z, where each component induces longitudinal NCT individually. For instance, magnetic field $B_x\mathbf{x} + B_y\mathbf{y}$ in materials with $422.1'$ MPG is superposed by B_x and B_y, yielding longitudinal NCT along the x and y directions.

[61] Z. Zhou, G. Cao, J. Liu, and H. Liu, npj Comput. Mater. **6**, 149 (2020).

[62] L. Tao and E. Y. Tsymbal, npj Comput. Mater. **6**, 172 (2020).

[63] Magndata, http://webbdcrista1.ehu.es/magndata.

[64] J. L. García-Muñoz, A. Romaguera, F. Fauth, J. Nogués, and M. Gich, Chem. Mater. **29**, 9705 (2017).

[65] M. Gich, C. Frontera, A. Roig, E. Taboada, E. Molins, H. R. Rechenberg, J. D. Ardisson, W. A. A. Macedo, C. Ritter, V. Hardy, J. Sort, V. Skumryev, and J. Nogués, Chem. Mater. **18**, 3889 (2006).

[66] Y. Wang, P. Wang, H. Wang, B. Xu, H. Li, M. Cheng, W. Feng, R. Du, L. Song, X. Wen, X. Li, J. Yang, Y. Cai, J. He, Z. Wang, and J. Shi, Adv. Mater. **35**, 2209465 (2022).

[67] K. Xu, J. S. Feng, Z. P. Liu, and H. J. Xiang, Phys. Rev. Appl. **9**, 044011 (2018).

[68] The nonzero $\sigma^{(2)}_{xxx}$ at $\mu = 0$ eV comes from the thermal smearing, which is incorporated by setting the temperature as 300 K in the Fermi-Dirac distribution.

[69] C. Wang, Y. Gao, and D. Xiao, Phys. Rev. Lett. **127**, 277201 (2021).

[70] H. Liu, J. Zhao, Y.-X. Huang, W. Wu, X.-L. Sheng, C. Xiao, and S. A. Yang, Phys. Rev. Lett. **127**, 277202 (2021).

[71] V. T. Pham, I. Groen, S. Manipatruni, W. Y. Choi, D. E. Nikonov, E. Sagasta, C.-C. Lin, T. A. Gosavi, A. Marty, L. E. Hueso, I. A. Young, and F. Casanova, Nat. Electron. **3**, 309 (2020).

[72] P. Němec, M. Fiebig, T. Kampfrath, and A. V. Kimel, Nat. Phys. **14**, 229 (2018).

[73] T. Jungwirth, X. Marti, P. Wadley, and J. Wunderlich, Nat. Nanotechnol. **11**, 231 (2016).

[74] J. Godinho, H. Reichlová, D. Kriegner, V. Novák, K. Olejník, Z. Kašpar, Z. Šobáň, P. Wadley, R. P. Campion, R. M. Otxoa, P. E. Roy, J. Železný, T. Jungwirth, and J. Wunderlich, Nat. Commun. **9**, 4686 (2018).

[75] Z.-F. Zhang, Z.-G. Zhu, and G. Su, Natl. Sci. Rev. **10**, nwad104 (2023).